JGR Solid Earth

RESEARCH ARTICLE
10.1029/2025JB032870

Olivine-Ahrensite Phase Relations in the Mg_2SiO_4-Fe_2SiO_4 System as a Function of Temperature

Artem Chanyshev[1], Dmitry Bondar[1], Lin Wang[1,2], Hongzhan Fei[3], Noriyoshi Tsujino[4], Yunke Song[1], Naira Martirosyan[1], Amrita Chakraborti[1,5], Eun Jeong Kim[1,6], Hu Tang[1,7], Shrikant Bhat[8], Robert Farla[8], and Tomoo Katsura[1]

[1]Bayerisches Geoinstitut (BGI), University of Bayreuth, Bayreuth, Germany, [2]Institute of Geochemistry, Chinese Academy of Science, Guiyang, China, [3]School of Earth Sciences, Zhejiang University, Hangzhou, China, [4]Japan Synchrotron Radiation Research Institute, Sayo, Japan, [5]University Lille, CNRS, INRAE, Centrale Lille, UMR 8207—UMET—Unité Matériaux et Transformations, Lille, France, [6]Department of Geoenvironmental Sciences, Kongju National University, Kongju, Korea, [7]State Key Laboratory of High Pressure and Superhard Materials, College of Physics, Jilin University, Changchun, China, [8]Deutsches Elektronen-Synchrotron DESY, Hamburg, Germany

Abstract Olivine and ahrensite are the primary components of the interiors of Fe-rich terrestrial planets and meteorites, making their phase relations crucial for planetary science. Moreover, their phase relations can be used for calibrating large-volume high-pressure devices such as multi-anvil apparatus. Here we defined the olivine–ahrensite phase relations in the MgO-FeO-SiO_2 system at 7.5–12.0 GPa at 1,530 and 1,950 K using a multi-anvil apparatus. Combining the current results with our previously determined binary loop at 1,740 K, we re-estimated the shock parameters of several L5 and L6-types meteorites. Also, we determined the olivine-ahrensite phase ratio and compositions along cold and warm Mars aerotherms for Mg/(Mg + Fe) ratios of 0.75 and 0.80. Using this mineralogical model, we estimated and compared seismic wave velocity profiles in Mars' interior to data from the InSight geophysical mission.

Plain Language Summary Olivine $(Mg,Fe)_2SiO_4$ is among the most abundant minerals in the interiors of terrestrial planets. In Earth's mantle it is predominantly magnesium-rich, whereas on other planets, such as Mars, it tends to be more Fe-rich. At greater depths, Fe-rich olivine transforms into a high-pressure spinel-structured phase known as ahrensite. Understanding the phase relations of these major mantle minerals is essential for constraining planetary structure and dynamics, making detailed studies of the olivine–ahrensite transition particularly important for iron-rich planets. Coexistence of olivine and ahrensite has also been observed in numerous meteorites. Based on the olivine–ahrensite phase relations, shock conditions of these meteorites can be estimated. In this study, we examined the high-pressure, high-temperature phase relations between olivine and ahrensite across a range of temperatures. We then used these results to estimate shock conditions in several meteorites and to construct a mineralogical model of Mars' interior. Based on this mineralogical model, we estimated and compared seismic wave velocity profiles in Mars' mantle to data from the InSight geophysical mission.

Key Points:

- Olivine-ahrenite binary loop was constructed at 1,530 and 1,950 K at 7.5–12.0 GPa
- Shock parameters of L5 and L6-types chondrites were calculated precisely
- Seismic wave velocity profiles along Mars' aerotherms were calculated and compared with the seismological data from the InSight mission

Supporting Information:

Supporting Information may be found in the online version of this article.

Correspondence to:

A. Chanyshev,
artem.chanyshev@uni-bayreuth.de

Citation:

Chanyshev, A., Bondar, D., Wang, L., Fei, H., Tsujino, N., Song, Y., et al. (2026). Olivine-ahrensite phase relations in the Mg_2SiO_4-Fe_2SiO_4 system as a function of temperature. *Journal of Geophysical Research: Solid Earth*, *131*, e2025JB032870. https://doi.org/10.1029/2025JB032870

Received 28 AUG 2025
Accepted 19 DEC 2025

Author Contributions:

Conceptualization: Artem Chanyshev
Formal analysis: Artem Chanyshev
Funding acquisition: Tomoo Katsura
Investigation: Artem Chanyshev, Lin Wang, Noriyoshi Tsujino, Yunke Song, Naira Martirosyan, Amrita Chakraborti, Eun Jeong Kim, Hu Tang, Shrikant Bhat, Robert Farla
Methodology: Artem Chanyshev, Dmitry Bondar, Tomoo Katsura
Software: Hongzhan Fei
Supervision: Artem Chanyshev, Tomoo Katsura
Validation: Artem Chanyshev
Writing – original draft: Artem Chanyshev

1. Introduction

Olivine polymorphs are believed to be the main constituents of the interiors of rocky planets. These polymorphs are believed to have an Mg# = Mg/(Mg + Fe) = 0.9 in the Earth's mantle, and their phase relations are well studied for the compositions close to this Mg# (e.g., Chanyshev et al., 2022). However, in the Martian mantle, olivine may be more Fe-enriched than in the Earth's mantle and has Mg# = 0.75–0.80 (Khan et al., 2018). Moreover, beyond our solar system, astronomers have discovered numerous terrestrial exoplanets that may be even more enriched in Fe than Mars, and in their mantles, olivine may have Mg# = 0.55 (McDonough & Sun, 1995). Therefore, understanding the phase relations of the Fe-rich olivine polymorphs over a broad range of pressures, temperatures, and iron content is necessary for modeling the interior structure and dynamics of Fe-enriched exoplanets.

Olivine (α-$(Mg,Fe)_2SiO_4$) transforms into a spinel-structured phase (γ-$(Mg,Fe)_2SiO_4$) at high pressures (Ringwood, 1958). γ-Mg_2SiO_4 and γ-$(Mg_{0.46}Fe_{0.54})_2SiO_4$ have been named ringwoodite (Binns et al., 1969) and ahrensite (Ma et al., 2016), respectively. In the mineralogical terminology, α- and γ-$(Mg,Fe)_2SiO_4$ containing 50 or more mol% of Mg_2SiO_4 are named forsterite and ringwoodite, respectively. The α- and γ-$(Mg,Fe)_2SiO_4$

Writing – review & editing: Artem Chanyshev, Dmitry Bondar, Lin Wang, Hongzhan Fei, Noriyoshi Tsujino, Yunke Song, Naira Martirosyan, Amrita Chakraborti, Eun Jeong Kim, Hu Tang, Shrikant Bhat, Robert Farla

containing less then 50 mol% of Mg_2SiO_4 are named fayalite and ahrensite, respectively. However, since most of γ-$(Mg,Fe)_2SiO_4$ in this study contains less than 50 mol% Mg_2SiO_4, we consistently refer to it as ahrensite throughout this paper. Previous experimental studies revealed that olivine and ahrensite form a binary loop at high pressures and temperatures. A pioneering experimental study by Akimoto and Fujisawa (1968) determined this binary loop at 1,073, 1,273, and 1,473 K. It should be noted that modern techniques for determining pressure, identifying phases and measuring compositions were unavailable or impractical when Akimoto and Fujisawa conducted their study. Akaogi et al. (1989) later derived a phase diagram of the transition from high-temperature solution calorimetry data. Frost (2003) determined these phase relations at 1,673 K. The most recent data were provided by Chanyshev et al. (2021) at 1,740 K, where the binary loop was determined using advanced multi-anvil techniques. These techniques include determining pressure and identifying phases using in situ X-ray diffraction (XRD) and analyzing phase compositions of recovered run products using an electron probe microanalyzer.

The olivine–ahrensite phase relations are also important for meteoritics, since both phases are present in meteorites, and ahrensite is formed via solid-state transformation of olivine during an impact event. Based on the olivine–ahrensite binary loop, one can estimate the shock parameters of meteorite impact. Chanyshev et al. (2021) attempted to estimate these parameters for several meteorites, but some of these estimations may contain significant uncertainties because the binary loop was determined only at 1,740 K. The authors provided a tool to estimate pressure and temperature simultaneously based on the compositions of coexisting olivine and ahrensite, but it works only in a limited temperature range. To extend this range, we investigated the temperature dependence of the olivine-ahrensite transition as a function of pressure by determining the binary loop at different temperatures.

2. Experimental Procedure

2.1. Sample Preparation

The starting materials used in this study were similar to those in Chanyshev et al. (2021). We used $(Mg_x, Fe_{1-x})_2SiO_4$ starting compositions in the range of $(Mg_{0.80}Fe_{0.20})_2SiO_4$ (Fo80)-$(Mg_{0.10}Fe_{0.90})_2SiO_4$ (Fo10). These solid solutions were synthesized from SiO_2, MgO, and Fe_2O_3 oxides. Prior to use, SiO_2 and MgO were annealed at 1,270 K and Fe_2O_3 at 770 K for 16 hr. The dried powders were then stored overnight in a vacuum furnace at 370 K, weighed, and mixed in appropriate proportions. Each mixture was ground with acetone for 1 hr, pressed into pellets, and sintered for 20 hr in a CO–CO_2 gas-mixing furnace at 1,370–1,420 K at fO_2 = IW + 2. We repeated this procedure a few times for each starting material until powder XRD analyses confirmed the absence of secondary phases.

An MgO powder mixed with a diamond powder (10:1 wt.%) was used as a pressure marker for in situ XRD experiments. The MgO powder was heated at 1,270 K for 16 hr prior to weighing. The mixture was ground with acetone for 1 hr.

The mixture of MgO and diamond was sintered by compressing to 5 GPa and heated to 1,000 K for 1 hr using a multi-anvil press at Bayerisches Geoinstitut, University of Bayreuth. WC anvils with a truncated edge length of 15.0 mm were used for this sintering. Experimental cell contained Cr_2O_3-doped MgO pressure medium and stepped cylindrical graphite heater. Sample was encapsulated in a 50-μm thick Mo foil. A $W_{97}Re_3$−$W_{75}Re_{25}$ thermocouple was used to measure the sample temperature. The sintered olivine solid solutions and mixture of MgO and diamond were then cut into disks with a diameter of 1 mm and a height of 0.3 mm.

2.2. High-Pressure High-Temperature Experiment With In Situ X-ray diffraction

We performed several in situ high-pressure multi-anvil experiments at the Deutsches Elektronen-Synchrotron (DESY) using the 3 × 5 MN six-ram multi-anvil press (Farla et al., 2022). We employed energy-dispersive XRD with a Ge SSD (4096-channel MCA) and CCD imaging. The SSD-MCA was calibrated using the γ-ray lines of different metals (^{57}Co and ^{133}Ba) before the measurements. 2θ diffraction angle was defined with a high precision of 0.0001° before each experiment, using MgO and SRM-660c LaB_6 (Black et al., 2020) calibrants at ambient conditions as standard references.

We used a cell assembly similar to that used by Chanyshev et al. (2021). The cell assembly contained Cr_2O_3-doped MgO pressure medium, a strip-type boron-doped diamond heater (Xie et al., 2017, 2020), MgO sample capsule, Mo electrodes, and ZrO_2 thermo-insulators. Temperature was measured with a $W_{97}Re_3$–$W_{75}Re_{25}$ thermocouple, with corrections also applied for pressure effects on the thermoelectromotive force (Nishihara et al., 2020). Samples and pressure marker discs were placed in the assembly center. These discs were separated from one another by 25-μm thick Re foils. Typically, four samples with different compositions were loaded in each assembly.

The experimental procedure is described as follows. First, the cell assembly was compressed and then heated to the target pressure and temperature conditions. In the current project, the target temperatures before correction were 1,500 and 1,900 K, and after correction were ≈1,530 and ≈1,950 K. The target pressure was kept constant by changing the multi-anvil press load. In 20 min at the target temperature, the sample was quenched. Before decompression, the phase composition of the quenched run products was detected by XRD.

The incident X-ray beam was collimated to 0.3 and 0.05 mm in the vertical and horizontal dimensions, respectively. During XRD measurements, the press was oscillated around the vertical axis from 0° to 4° to reduce intensity heterogeneities in the diffracted signals. In each experiment, at a given pressload and temperature, the unit cell volume of the MgO calibrant was measured, and pressures were calculated using the third-order Birch–Murnaghan and Vinet equations of state (Tange et al., 2009). In the manuscript, we provide the average pressure values from these two equations of state.

2.3. Sample Analysis

Cross-sections of the recovered samples were prepared and further analyzed by scanning electron microscopy (SEM). Backscattered electron (BSE) images were taken on the cross sections. The phases present on the cross sections were examined by an energy-dispersive detector.

The chemical compositions of olivine and ahrensite were obtained using a JEOL JXA-8200 electron probe microanalyzer (EPMA), which was operated at 15 kV and 5 nA. Calibration standards of enstatite were employed for Mg and Si, and metallic iron for Fe. Oxygen content was derived from stoichiometry. Grains near the edges of the samples were avoided.

3. Results and Discussion

3.1. Run Products

The XRD measurements revealed α-$(Mg,Fe)_2SiO_4$ and γ-$(Mg,Fe)_2SiO_4$ at 8.27(6)–11.68(3) GPa at ≈1,530 K and at 9.54(13)–11.98(4) GPa at ≈1,950 K (Figure 1). Some XRD patterns also contain reflections of the surrounding MgO from the pressure media. The SEM and EPMA analysis show the coexistence of two phases with olivine stoichiometry and different Fe/Mg ratios (Figure 2a). We therefore consider that the Mg-enriched phase is olivine, and the Fe-enriched phase is ahrensite.

At 12.88(5) GPa and 1,960 K, we observed the coexistence of wadsleyite and ahrensite by XRD. The SEM analyses showed the coexistence of two phases with olivine stoichiometry and different Fe/Mg ratios. Based on the topology of the $(Mg,Fe)_2SiO_4$ phase diagram at high pressure (Frost, 2003), the Mg-enriched phase is wadsleyite, and the Fe-enriched phase is ahrensite.

Table 1 shows the composition of coexisting phases based on the EPMA analyses. At 1,530 K, the Mg_2SiO_4 component increases from 0.47 to 0.86 in olivine and from 0.19 to 0.64 in ahrensite with increasing pressure from 8.27(6) to 11.68(3) GPa. At 1,950 K, the Mg_2SiO_4 component rises from 0.54 to 0.73 in olivine and from 0.32 to 0.46 in ahrensite with increasing pressure from 9.54(13) to 11.98(4) GPa. The Mg_2SiO_4 contents in coexisting wadsleyite and ahrensite at 1,960 K and 12.88(5) GPa were determined as 0.66 and 0.56, respectively.

In the current study, we assume that all Fe in both olivine and ahrensite is ferrous, although we did not conduct Mössbauer measurements of recovered run products and did not control oxygen fugacity conditions, as it was done in Frost (2003) by adding metallic Fe to the starting material. Potentially, ahrensite or ringwoodite may incorporate some amount of ferric Fe, but in dry systems, Fe^{3+} content is typically low (≈3% of total Fe), since there is limited charge compensation without hydrogen (McCammon et al., 2004). Another evidence of reduced condition in the current study is that the sum of cations is 2.98–3.00 for four oxygen atoms (Table 1), assuming

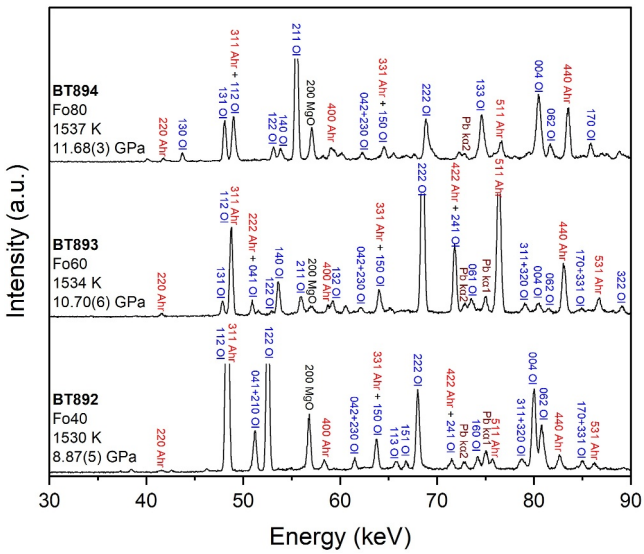

Figure 1. Olivine-ahrensite coexistence confirmed by X-ray diffraction in BT892, BT893, and BT894 experimental runs. From the left side, run number, starting material, and experimental parameters are shown. The blue, red, and black numbers show the Miller indices of olivine, ahrensite, and periclase, respectively. The fluorescence lines of Pb Kα and Kβ are shown by the Siegbahn notation.

that all Fe is ferrous. If our samples contained significant amounts of ferric iron, the total cation sum should have been greater than 3.

3.2. Thermodynamic Approach

The thermodynamic approach used in the current study is similar to that in Chanyshev et al. (2021). Here we briefly describe this approach:

The partitioning of Fe and Mg between the coexisting olivine and ahrensite are described by the exchange reactions:

$$MgSi_{0.5}O_2(\alpha) = MgSi_{0.5}O_2(\gamma), \quad (1)$$

$$FeSi_{0.5}O_2(\alpha) = FeSi_{0.5}O_2(\gamma), \quad (2)$$

At equilibrium and at a fixed pressure and temperature the standard state Gibbs free energy change for reactions (1) and (2) are:

$$\Delta G_{MgSi_{0.5}O_2}(P,T) = \Delta H^0_{MgSi_{0.5}O_2} - T\Delta S^0_{MgSi_{0.5}O_2} + \int_0^P \Delta V_{MgSi_{0.5}O_2}(P,T) + RT\ln\frac{X^{Ahr}_{MgSi_{0.5}O_2}}{X^{Ol}_{MgSi_{0.5}O_2}} + W^{Ahr}\left(1 - X^{Ahr}_{MgSi_{0.5}O_2}\right)^2 - W^{Ol}\left(1 - X^{Ol}_{MgSi_{0.5}O_2}\right)^2 \quad (3)$$

$$\Delta G_{FeSi_{0.5}O_2}(P,T) = \Delta H^0_{FeSi_{0.5}O_2} - T\Delta S^0_{FeSi_{0.5}O_2} + \int_0^P \Delta V_{FeSi_{0.5}O_2}(P,T) + RT\ln\frac{X^{Ahr}_{FeSi_{0.5}O_2}}{X^{Ol}_{FeSi_{0.5}O_2}} + W^{Ahr}\left(1 - X^{Ahr}_{FeSi_{0.5}O_2}\right)^2 - W^{Ol}\left(1 - X^{Ol}_{FeSi_{0.5}O_2}\right)^2 \quad (4)$$

Where $\Delta H^0_{MgSi_{0.5}O_2}$ and $\Delta H^0_{FeSi_{0.5}O_2}$ are the enthalpy changes in reactions (1) and (2) at 1 atm, $\Delta S^0_{MgSi_{0.5}O_2}$ and $\Delta S^0_{FeSi_{0.5}O_2}$ are the entropy change in reactions (1) and (2) at 1 atm, $\Delta V_{MgSi_{0.5}O_2}(P,T)$ and $\Delta V_{FeSi_{0.5}O_2}(P,T)$ are the volume changes at a pressure of P and temperature of T, and W^N is the Margules interaction parameter that quantifies the non-ideal behavior of solid solutions.

The molar volumes pressure and temperature dependence of the $MgSi_{0.5}O_2$ forsterite and ringwoodite as well as $FeSi_{0.5}O_2$ fayalite and ringwoodite have been determined previously by Jacobs et al. (2001), Katsura et al. (2004, 2009). The $\Delta V_{MgSi_{0.5}O_2}$ and $\Delta V_{FeSi_{0.5}O_2}$ values at 1,530 and 1,950 K and various pressures are calculated from the endmember's molar volumes.

$\Delta S^0_{MgSi_{0.5}O_2}$, $\Delta S^0_{FeSi_{0.5}O_2}$, $\Delta H^0_{MgSi_{0.5}O_2}$, $\Delta H^0_{FeSi_{0.5}O_2}$, W^{Ol}, and W^{Ahr} were calculated by simultaneous least square fitting of the current experimental data and data from Chanyshev et al. (2021), assuming that, $\Delta G_{MgSi_{0.5}O_2}$ and $\Delta G_{FeSi_{0.5}O_2}$ equal 0 at equilibrium: $\Delta S^0_{MgSi_{0.5}O_2} = -7.753$ J/mol, $\Delta S^0_{FeSi_{0.5}O_2} = -11.727$ J/mol, $\Delta H^0_{MgSi_{0.5}O_2} = 14.356$ kJ/mol; $\Delta H^0_{FeSi_{0.5}O_2} = -4.986$ kJ/mol; $W^{Ol} = 2.037$ kJ/mol; and $W^{Ahr} = 2.697$ kJ/mol.

Using the obtained data, we updated the software (olivine–ahrensite loop calculation tool) created by our research group and attached to Chanyshev et al. (2021). The updated software can be used to determine pressure in the temperature range of 1,200–2,300 K from the compositions of coexisting olivine and ahrensite.

3.3. Phase Diagram

Figure 3 illustrates the phase relations in the Mg_2SiO_4-Fe_2SiO_4 system at 5.0–12.0 GPa at 1,530, 1,740 and 1,950 K based on our thermodynamic calculations. With increasing temperature, the binary loop shifts to higher pressure. Our data at 1,530 K are in good agreement with our calculated loop at 1,530 K, whereas our data at 1,950 K slightly differ at high pressures from the computed loop at 1,950 K (Figure 3). At 1,950 K, we also

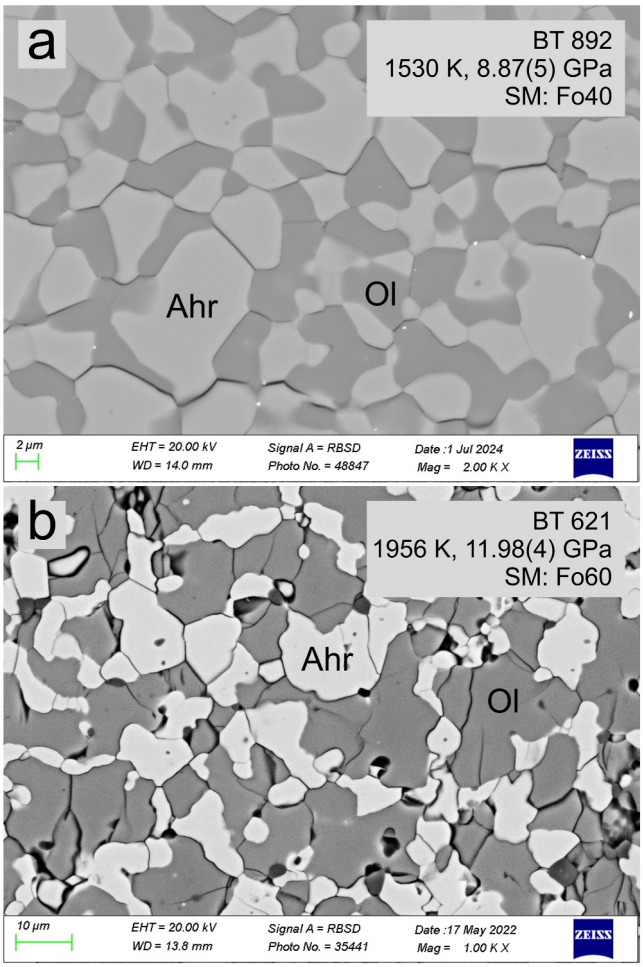

Figure 2. Backscattered scanning electron microscopy images of run products from experiments (a) BT892 at 1,530 K and 8.87(5) GPa and (b) BT621 at 1,956 K and 11.98(4) GPa.

observed coexistence of wadsleyite and ahrensite at 12.88 GPa, which allows us to determine the upper part of the olivine-ahrensite binary loop and propose the position of the wadsleyite-ahrensite binary loop (Figure 3).

Comparison of the calculated olivine-ahrensite binary loops at 1,530 and 1,950 K with previous experimental results at similar temperatures is shown in Figure 4. Akimoto (1987) and Frost (2003) constructed binary loops at 1,473 and 1,673 K, respectively, based on high-pressure experimental data. Akaogi et al. (1989) calculated loops at 1,473 and 1873 K using calorimetric measurements at ambient pressure. The left parts of our determined loops at 1,530 and 1,950 K, corresponding to the compositions of olivine, are in good agreement with previous results from Akimoto (1987) and Akaogi et al. (1989) at 1,473 and 1,873 K (Figure 4). In contrast, the right parts of the loops at 1,530 and 1,950 K, representing the compositions of ahrensite, show significant discrepancies compared to the previous data from Akimoto (1987) and Akaogi et al. (1989) at 1,473 and 1,873 K (Figure 4). Therefore, our determined loops are narrower than those by Akimoto (1987) and Akaogi et al. (1989). Moreover, their determined upper part of loops, separating the wadsleyite stability field, are located at higher pressures than our proposed boundaries.

The binary loop determined by Frost (2003) was compared with the loop calculated at 1673 K using our software (Figure S1). The experimental data points reported by Frost (2003) are located about 0.5 GPa lower than the loop calculated by him, and about 0.7 GPa higher than predicted by our thermodynamic model. Possibly, this discrepancy is caused by the overestimation of pressure conditions in Frost (2003) experiments. For the multi-anvil press calibration, he used the post-spinel phase transition determined by Katsura et al. (1998). Recently, this phase transition was re-investigated by Akaogi et al. (2023), and the newly re-determined boundary is located about 1–2 GPa lower than that proposed by Katsura et al. (1998). The widths of binary loops calculated by Frost (2003) and by us are almost the same.

The observed discrepancies between our data and Akimoto (1987) can be explained by the different analytical methods used to determine the binary loop parameters. Akimoto (1987) used XRD to define the phases in recovered samples without compositional analyses. In a phase diagram where one of the axes is the composition of the coexisting phases, such a method is not able to determine the loop parameters accurately. The calculated olivine–ahrensite loops from Akaogi et al. (1989) at 1,473 and 1,873 K seem to be wider than ours at 1,530 and 1,950 K, and these discrepancies could be caused by using different Margules parameters. Frost (2003) calculated the loop using the same procedure as Akaogi et al. (1989), but with different interaction parameters. While Akaogi et al. (1989) derived their parameters by fitting calorimetric data obtained at ambient pressure and high temperature, Frost (2003) determined his parameters by fitting experimental data collected at high pressures and temperatures, similar to our study. As a result, Frost (2003) obtained a narrower loop than those from Akaogi et al. (1989), and its width is comparable to those determined in the current study.

3.4. Large-Volume High-Pressure Devices Calibration

The defined olivine-ahrensite phase relations can be applied for in-house pressure calibration of large-volume high-pressure devices such as multi-anvil apparatus at high temperature, as we proposed in Chanyshev et al. (2021). The method can be briefly described as follows: several pieces of $(Mg,Fe)_2SiO_4$ samples with different Mg/Fe ratios should be placed in the cell assembly chamber near the sample. Under experimental conditions, at least one sample should have the coexistence of olivine and ahrensite, while the others may show a single phase of either olivine or ahrensite. Recovered samples should be analyzed by EPMA to obtain olivine and ahrensite compositions. Using the updated software, sample pressure can be estimated by the compositions of the coexisting olivine and ahrensite. Reliability of this calibration was confirmed by comparing of experimental

Table 1
Experimental Run Conditions and Electron Probe Microanalyzer Data

Sample		Temperature, K after P-correction of EMF	Pressure, GPa after P-correction of EMF	Starting material	Ahrensite composition (light)					Olivine composition (dark)				
					Mg^{2+}	Fe^{2+}	Si^{4+}	Sum of cations	Mg#	Mg^{2+}	Fe^{2+}	Si^{4+}	sum of cations	Mg#
BT892	Average	1,530	8.87	Fo40	0.58	1.40	1.01	2.99	0.29	1.24	0.76	1.00	3.00	0.62
	St. dev		0.05		0.01	0.01	0.00	0.00		0.01	0.01	0.00	0.00	
BT893	Average	1,534	10.70	Fo60	1.00	0.99	1.00	3.00	0.50	1.58	0.43	0.99	3.01	0.79
	St. dev		0.06		0.02	0.02	0.00	0.00		0.04	0.04	0.00	0.00	
BT894	Average	1,537	11.68	Fo80	1.28	0.72	1.00	3.00	0.64	1.73	0.28	0.99	3.01	0.86
	St. dev		0.03		0.03	0.02	0.01	0.01		0.02	0.02	0.00	0.00	
BT895	Average	1,529	8.27	Fo40	0.38	1.59	1.01	2.99	0.19	0.94	1.06	1.00	3.00	0.47
	St. dev		0.06		0.00	0.00	0.00	0.00		0.03	0.03	0.00	0.00	
BT614[a]	Average	1,958	12.88	Fo60	1.12	0.87	1.00	3.00	0.56	1.31	0.69	1.00	3.00	0.66
	St. dev		0.05		0.01	0.00	0.00	0.00		0.00	0.00	0.00	0.00	
BT621	Average	1,956	11.98	Fo60	0.91	1.07	1.01	2.99	0.46	1.46	0.55	0.99	3.00	0.73
	St. dev		0.04		0.01	0.01	0.00	0.00		0.02	0.02	0.00	0.00	
BT641	Average	1,951	10.61	Fo40	0.70	1.26	1.02	2.98	0.36	1.26	0.73	1.00	3.00	0.64
	St. dev		0.06		0.00	0.00	0.00	0.00		0.02	0.02	0.00	0.00	
BT638	Average	1,948	9.54	Fo40	0.63	1.37	1.00	3.00	0.32	1.09	0.91	1.00	3.00	0.54
	St. dev		0.13		0.01	0.01	0.00	0.00		0.01	0.02	0.00	0.00	

[a]In the BT614 run, the wadsleyte composition was shown in the column «Olivine composition (dark)».

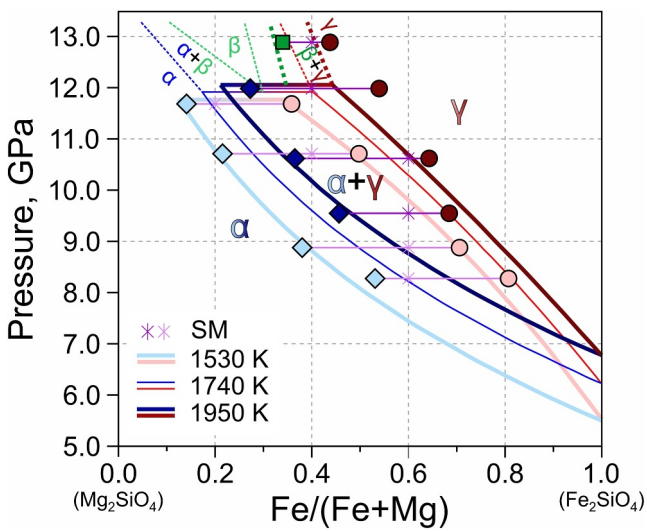

Figure 3. Experimental data and calculated olivine-ahrensite loops. Blue diamonds, red circles, and green squares represent the compositions of olivine (α), ahrensite (γ), and wadsleyite (γ), respectively. Purple stars indicate compositions of starting materials. Optimized thermodynamic data at 1,530, 1,740 and 1,950 K are shown as solid colored curves. Optimized thermodynamic data at 1,740 K are shown as thinner curves than the data at 1,530 and 1,950 K. Pressure determination errors are smaller than the symbols.

pressure values from the current study and Chanyshev et al. (2021) with those calculated using our software at 1,530, 1,740 and 1,950 K (Table 2). At 1530 K, observed residuals are relatively small (0.04–0.08 GPa), except for the data point at the lowest studied pressure, where the difference is 0.40 GPa. At 1,740 K, the residuals are between 0.08 and 0.30 GPa, and at 1,950 K, the residuals are 0.18–0.66 GPa. We consider that these residuals can be caused by experimental uncertainties, which cannot be avoided. Additional experiments at 1,950 K are required to establish a more precise thermodynamic model at this temperature. We estimated residual variance s^2 between our experimental and model data using the following formula:

$$s^2 = \frac{1}{N-p}\sum_{i=1}^{N} r_i^2 \quad (5)$$

Where n is the number of data points, p is the number of fitted parameters, and r_i is the residual between experimental and predicted values. Standard deviation of the fit, which indicates the model's predictive uncertainty, is the square root of the residual variance. The calculated residual variance and standard deviation are 0.15 and 0.39, respectively. Thus, the uncertainty in determining the pressure parameters using our model is 0.39 GPa. Moreover, based on the comparison of the residuals at different temperatures, the proposed multi-anvil calibration method is primarily applicable to experiments up to 1,740 K and should be used with caution at higher temperatures.

3.5. Determination of Shock Parameters

Some meteorites have characteristic mineral associations that help to determine the impact conditions, and the olivine-ahrensite assemblage is one of

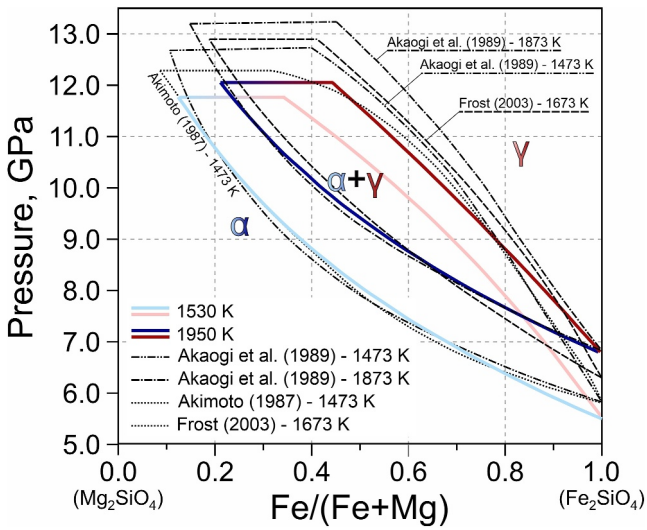

Figure 4. Comparison of our results with previous data (Akaogi et al., 1989; Akimoto, 1987; Frost, 2003). Optimized thermodynamic data at 1,530 and 1,950 K are shown as solid colored curves. Data from Frost (2003) at 1,673 K are shown by black dashed curves, data from Akimoto (1987) at 1,472 K are shown by black dotted curves, data from Akaogi et al. (1989) at 1,473 and 1,873 K are shown by black double-dash-dotted and dash-dotted curves, respectively.

them (e.g., Acosta-Maeda et al., 2013; Baziotis et al., 2018; Ma et al., 2016; Miyahara et al., 2010; Pittarello et al., 2015; Sharp et al., 2019; Walton & McCarthy, 2017). These impact conditions are typically estimated from the compositions of coexisting minerals such as olivine and ahrensite using their phase relations. These estimates assume that these minerals are in equilibrium, as indicated by the compositional differences between them. If the transformation occurs under non-equilibrium conditions, the transformation would proceed without any change in composition (Sharp & DeCarli, 2006). In Chanyshev et al. (2021), we estimated shock parameters of several Martian meteorites and chondrites. However, some of these estimations contain significant uncertainties, as in Chanyshev et al. (2021), the olivine-ahrensite phase relations were determined only at 1,740 K and then extrapolated to lower and higher temperatures. In the current study, we determined the olivine-ahrensite phase relations as a function of temperature, enabling application of our results to a wide range of temperatures. Re-estimated shock conditions of Martian meteorites Tissint (Ma et al., 2016) and NWA 8159 (Sharp et al., 2019) exceed 2,300 K and are 11.47(44) and 9.42(61) GPa (Table 3). Shock conditions of L5-type chondrites Taiban (Acosta-Maeda et al., 2013) and Dhofar 1970 (Walton & McCarthy, 2017) were re-estimated as 1,300 K and 11.51(1) GPa and 1,200 K and 10.06(1) GPa, respectively (Table 3). Shock conditions of L6-type chondrites Asuka-09584 (Pittarello et al., 2015) and Château-Renard (Baziotis et al., 2018) were re-estimated as 1,575(5) K and 11.37(1) GPa and 1,700 K and 11.44(0) GPa, respectively (Table 3). However, due to the model's predictive uncertainty being estimated as 0.39 GPa, we can adjust the pressure estimates to ±0.4 GPa (Table 3). Therefore, using our updated software, we can precisely determine shock parameters of L5- and L6- types meteorites. We were unable to determine the shock parameters of some Martian meteorites. In the Martian meteorite Tissint (Ma et al., 2016), ahrensite is located near the melt pocket and the bridgmanite + wustite + stishovite association, and therefore, the ahrensite could be formed via the bridgmanite + wustite + stishovite = ahrensite + wustite + stishovite phase transition occurring at 23–24 GPa (Ishii et al., 2019). In the Martian meteorite NWA 8159 (Sharp et al., 2019), ahrensite was formed on a margin between a shock vein and olivine with Mg# = 0.34. Based on our thermodynamic model, ahrensite coexisted with the olivine with Mg# = 0.34 should be more enriched in Fe than reported by Sharp et al. (2019). We assume that Fe diffused from the ahrensite to the minerals/melt in a bordering shock vein.

Table 2
Comparison of Pressure Values Determined Experimentally From the MgO Unit Cell Volumes and From the Thermodynamic Calculations

Run. No.	T (K) after correction	P (GPa) after correction	T (K) used for calculation	P (GPa) calculated at 1,530 and 1,950 K	$\lvert\Delta P\rvert$ (GPa)
BT892	1,530	8.87 (5)	1,530	8.93 (13)	0.06
BT893	1,534	10.70 (6)	1,530	10.62 (5)	0.08
BT894	1,537	11.68 (3)	1,530	11.64 (7)	0.04
BT895	1,529	8.27 (6)	1,530	7.87 (7)	0.40
HH310	1,745	11.19 (17)	1,740	11.27 (3)	0.08
HH300	1,743	10.34 (11)	1,740	10.47 (4)	0.13
HH311	1,738	9.18 (14)	1,740	9.41 (4)	0.23
HH312	1,735	8.25 (13)	1,740	8.55 (7)	0.30
HH314	1,733	7.48 (13)	1,740	7.62 (1)	0.14
BT621	1,956	11.98 (4)	1,950	11.32 (11)	0.66
BT641	1,951	10.61 (6)	1,950	10.43 (13)	0.18
BT638	1,948	9.54 (13)	1,950	9.84 (18)	0.30

Note. $\lvert\Delta P\rvert$ is the absolute difference between experimentally determined and thermodynamically calculated pressures at 1,530, 1,740, and 1,950 K. Experimental data at 1,733–1,745 K are given from Chanyshev et al. (2021).

Table 3
Shock Conditions of Several Meteorites

Meteorite	Type	Reference	Olivine	Ahrensite	T, K	P, GPa	[a]P, GPa
Tissint	Martian (shergottite)	Ma et al. (2016)	$Fo_{0.64}Fa_{0.36}$	$Rw_{0.46}Ahr_{0.54}$	>2,300	11.47 ± 0.44	
NWA 8159	Martian ([b]aug. basalt)	Sharp et al. (2019)	$Fo_{0.34}Fa_{0.66}$	$Rw_{0.26}Ahr_{0.74}$	>2,300	9.42 ± 0.61	
Taiban	L5	Acosta-Maeda et al. (2013)	$Fo_{0.92}Fa_{0.08}$	$Rw_{0.73}Ahr_{0.27}$	1,300	11.51 ± 0.01	11.5 ± 0.4
Dhofar 1970	L5	Walton and McCarthy (2017)	$Fo_{0.86}Fa_{0.14}$	$Rw_{0.54}Ahr_{0.46}$	1,200	10.06 ± 0.01	10.1 ± 0.4
Asuka-09584	L6	Pittarello et al. (2015)	$Fo_{0.83}Fa_{0.17}$	$Rw_{0.58}Ahr_{0.42}$	1,575 ± 5	11.37 ± 0.01	11.4 ± 0.4
Château-Renard	L6	Baziotis et al. (2018)	$Fo_{0.80}Fa_{0.20}$	$Rw_{0.55}Ahr_{0.45}$	1,700	11.44 ± 0.01	11.4 ± 0.4

Note. Olivine and ahrensite compositions are given as forsterite (Mg_2SiO_4)—fayalite (Fe_2SiO_4) and ringwoodite (Mg_2SiO_4)—ahrensite (Fe_2SiO_4) solid solutions. [a]P, GPa—pressure conditions, determined considering the model's predictive uncertainty. [b]Aug. basalt—augite basalt.

We would like to mention that the determined impact parameters for Martian and L5–L6 type meteorites may not represent peak shock conditions, as these meteorites contain high-pressure mineral phases, such as bridgmanite (Baziotis et al., 2018; Ma et al., 2016), maskelynite (Pittarello et al., 2015), or majorite garnet (Acosta-Maeda et al., 2013). Nevertheless, the currently obtained shock parameters are useful for constructing the pressure–temperature path after passing the peak pressure.

3.6. Mars' Mineralogy and Seismic Wave Velocities

Fe-rich olivine and its polymorphs are the main constituent minerals in rocky planets, and one of the most studied examples is Mars. Olivine in the Martian mantle is expected to have Mg# = 0.75 (Taylor, 2013) to 0.80 (Khan et al., 2022). Therefore, we can evaluate the proportion and composition of coexisting olivine and ahrensite for Mars' interiors and estimate how seismic velocities change with depth (Figure 5). We used adiabatic temperature profiles (aerotherms) calculated for olivine with Mg# = 0.75 and 0.80 by Wang et al. (2025). The adiabatic temperatures calculated for Fo75 olivine vary from 1,700 K at 5 GPa to 1,900 K at 18.5 GPa, and are about 150 K higher than those calculated for Fo80 olivine (Wang et al., 2025). Along the Mars' aerotherm, olivine with the composition of Fo75 gradually transforms to ahrensite from 11.2 GPa, reaching about 30% ahrensite by volume at 12.0 GPa. The Fe/(Fe + Mg) ratio in olivine and ahrensite gradually decreases from 0.25 and 0.51 to 0.18 and 0.41, respectively. Olivine with the composition of Fo80 gradually transforms to ahrensite from 11.4 GPa, and at 12.0 GPa, the volume of ahrensite becomes 25%. The Fe/(Fe + Mg) ratio in olivine and ahrensite gradually decreases from 0.20 and 0.44 to 0.15 and 0.34, respectively.

Based on the olivine and ahrensite ratio and composition of these phases, one can estimate the seismic wave velocity profiles in Mars' interior. Numerous studies considered that at a depth of 900–1,000 km, the $(Mg, Fe)_2SiO_4$ phase is represented solely by olivine (e.g., Yoshizaki and McDonough (2020)). Here, we calculated the V_p and V_s velocities for the olivine-ahrensite assemblage and pure olivines for Fo75 and Fo80 compositions along Mars adiabats (Figure 5). Elastic parameters for olivine and ahrensite-ringwoodite endmembers are given from Duffy et al. (1995), Graham et al. (1988), Kumazawa and Anderson (1969), Liu et al. (2008) and Matsui et al. (2006). Due to the gradual transition of olivine to ahrensite, both V_p and V_s increase in the region at 900–950 km depths more significantly than in the upper and lower regions of the Martian mantle. This variation is more prominent in V_s than in V_p. For example, the olivine-ahrensite assemblage has 1% and 4% higher V_p and V_s, respectively, compared to pure olivine in the Martian mantle.

Due to the limited seismological data obtained by the InSight space mission, the seismic wave velocity profiles on Mars are not as accurate as those on Earth. However, there are some calculated mineral physics models compared with P and S triplications, resulting from the interaction with a seismic discontinuity (Huang et al., 2022). We corrected these models assuming that olivine gradually transforms to ahrensite at around 900–950 km depth (Figure 6). Our corrected models indicate that there is almost no change in V_p velocity profile, while the V_s velocity profile becomes much steeper at these depths, although it is still within the low misfits of P and S triplications (Figure 6). More precise seismological data from space missions are required to evaluate the validity of our corrected model.

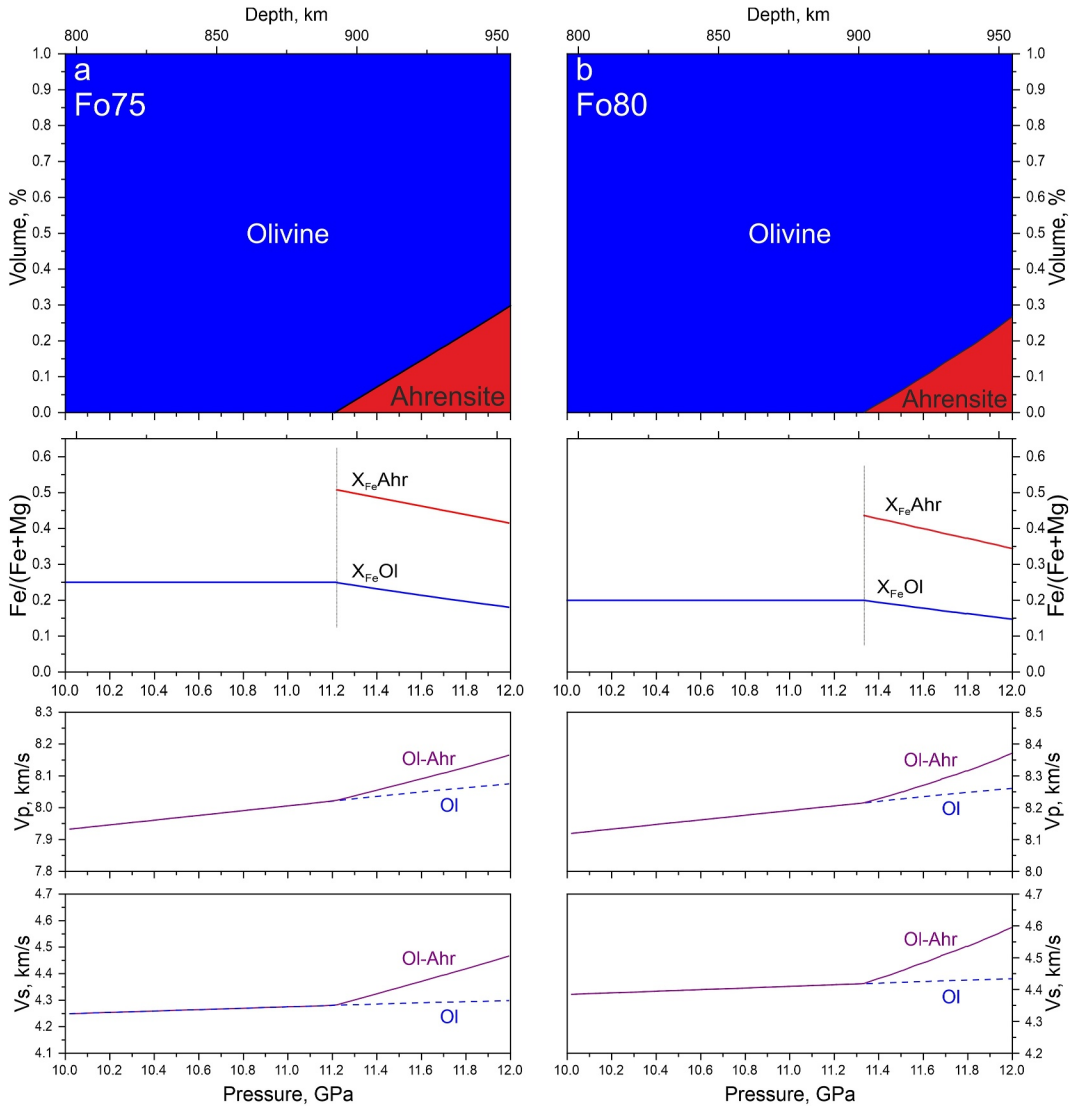

Figure 5. Olivine/ahrensite ratio (top), compositions of these olivine and ahrensite (middle), and seismic velocities (bottom) in two different compositional models of Mars, with Fo75 (Taylor, 2013) at left (a), and Fo80 (Khan et al., 2022) at right (b). Pressure and temperature conditions for these models are given from Wang et al. (2025). In the bottom graphs, V_p and V_s are calculated for pure olivine with Fo75 (left) and Fo80 (right) compositions (dashed blue lines) and for the olivine-ahrensite assemblage (solid purple curves) based on our thermodynamic calculations.

4. Conclusions

The olivine–ahrensite transition in the MgO-FeO-SiO_2 system was investigated at different temperatures of 1,530 and 1,950 K at 7.5–12.0 GPa using a combination of multi-anvil and in situ XRD techniques. At 1,530 K, the Mg_2SiO_4 component increases from 0.47 to 0.86 in olivine and from 0.19 to 0.64 in ahrensite with increasing pressure from 8.27(6) to 11.68(3) GPa. At 1,950 K, the Mg_2SiO_4 component rises from 0.54 to 0.73 in olivine and from 0.32 to 0.46 in ahrensite with increasing pressure from 9.54(13) to 11.98(4) GPa. At 1,960 K and 12.88(5) GPa, we observed the coexistence of wadsleyite and ahrensite. Combining our current results with those we obtained previously at 1,740 K (Chanyshev et al., 2021), we modified our previously developed software allowing pressure determination from the Mg/Fe ratio in coexisting olivine and ahrensite within an extended temperature range of 1,200–2,300 K. The thermodynamic model's predictive uncertainty is estimated as ±0.39 GPa. Using the software and considering the model's uncertainty, shock conditions of L5-type Taiban and Dhofar 1970 were re-determined as 1,300 K and 11.5(4) Gpa, and 1,200 K and 10.1(4) GPa, respectively, and L6-types chondrites Asuka-09584 and Château-Renard meteorites as 1,575(5) K and 11.4(4) Gpa, and 1,700 K

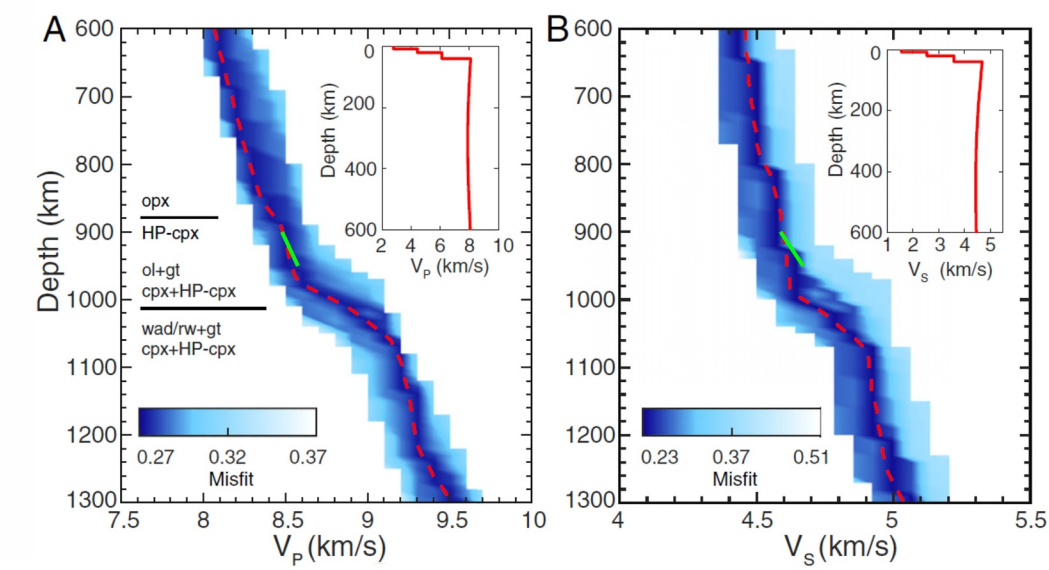

Figure 6. (redrawn from Figure 3 in Huang et al. (2022)). (a) V_p and (b) V_s profiles from mineral physics models colored by the misfits of P and S triplications, respectively. Solid green lines indicate the V_p (a) and V_s (b) profiles corrections assuming that olivine gradually transforms to ahrensite (for Fo75 composition). Opx—orthopyroxene, cpx—clinopyroxene, HP-cpx—high-pressure clinopyroxene, ol—olivine, gt—garnet, wad—wadsleyite, rw—ringwoodite.

and 11.4(4) GPa, respectively. Moreover, we calculated that in Mars' interior along cold and warm aerotherms, olivine with compositions Fo75 and Fo80 gradually transforms to ahrensite from 11.20 to 11.35 GPa to about 12 GPa, respectively, and the amount of ahrensite at 12 GPa is 25%–30% by volume. For Fo75, the Fe/(Fe + Mg) ratio in olivine and ahrensite gradually decreases from 0.25 and 0.51 to 0.18 and 0.41, respectively. For Fo80, the Fe/(Fe + Mg) ratio in olivine and ahrensite gradually decreases from 0.20 and 0.44 to 0.15 and 0.34, respectively. Based on these phase compositions and proportions, seismic wave velocity profiles along Mars' aerotherms were calculated and compared with the seismological data from the InSight mission.

Conflict of Interest

The authors declare no conflicts of interest relevant to this study.

Acknowledgments
We appreciate H. Fischer, S. Übelhack, R. Njul, U. Trenz, and S. Linhardt at the Bayerisches Geoinstitut and S. Sonntag at DESY for their technical assistance. This work was funded by the European Research Council (ERC) under the European Union's Horizon 2020 research and innovation program (Proposal No. 787 527) to T. Katsura. H. Fei acknowledges support from the National Key Research and Development Program of China (2024YFF0809700). We acknowledge DESY (Hamburg, Germany), a member of the Helmholtz Association HGF, for the provision of experimental facilities. Parts of this research were carried out at beamline P61B (Proposals No. I-20211514 and I-20231234). The beamline LVP instrument Aster-15 is funded by the ErUM-Pro programme (Grants 05K16WC2 and 05K13WC2) of the German Federal Ministry of Education and Research (BMBF). Open Access funding enabled and organized by Projekt DEAL.

Data Availability Statement

The developed software to calculate the olivine-ahrensite loop and instructions to use it are available at Chanyshev (2025b). The EPMA and XRD data, and SEM images for this paper are given at Chanyshev (2025a).

References

Acosta-Maeda, T. E., Scott, E. R., Sharma, S. K., & Misra, A. K. (2013). The pressures and temperatures of meteorite impact: Evidence from micro-Raman mapping of mineral phases in the strongly shocked Taiban ordinary chondrite. *American Mineralogist*, *98*(5–6), 859–869. https://doi.org/10.2138/am.2013.4300

Akaogi, M., Ito, E., & Navrotsky, A. (1989). Olivine-modified spinel-spinel transitions in the system Mg_2SiO_4-Fe_2SiO_4: Calorimetric measurements, thermochemical calculation, and geophysical application. *Journal of Geophysical Research*, *94*(B11), 15671–15685. https://doi.org/10.1029/jb094ib11p15671

Akaogi, M., Miyazaki, N., Tajima, T., & Kojitani, H. (2023). Post-spinel transition of Fe_2SiO_4 ahrensite at high pressure and high temperature. *Physics and Chemistry of Minerals*, *50*(3), 23. https://doi.org/10.1007/s00269-023-01247-4

Akimoto, S. I. (1987). High-pressure research in geophysics: Past, present and future. *High-Pressure Research in Mineral Physics: A Volume in Honor of Syun-iti Akimoto*, *39*, 1–13. https://doi.org/10.1029/gm039p0001

Akimoto, S. I., & Fujisawa, H. (1968). Olivine-spinel solid solution equilibria in the system Mg_2SiO_4-Fe_2SiO_4. *Journal of Geophysical Research*, *73*(4), 1467–1479. https://doi.org/10.1029/jb073i004p01467

Baziotis, I., Asimow, P. D., Hu, J., Ferrière, L., Ma, C., Cernok, A., et al. (2018). High pressure minerals in the Château-Renard (L6) ordinary chondrite: Implications for collisions on its parent body. *Scientific Reports*, *8*(1), 9851. https://doi.org/10.1038/s41598-018-28191-6

Binns, R., Davis, R., & Reed, S. (1969). Ringwoodite, natural $(Mg, Fe)_2SiO_4$ spinel in the Tenham meteorite. *Nature*, *221*(5184), 943–944. https://doi.org/10.1038/221943a0

Black, D. R., Mendenhall, M. H., Brown, C. M., Henins, A., Filliben, J., & Cline, J. P. (2020). Certification of Standard Reference material 660c for powder diffraction. *Powder Diffraction*, *35*(1), 17–22. https://doi.org/10.1017/s0885715620000068

Chanyshev, A. (2025a). Dataset for paper: Olivine-ahrensite phase relations in the Mg_2SiO_4-Fe_2SiO_4 system as a function of temperature [Dataset]. *Zenodo*. https://doi.org/10.5281/zenodo.17820460

Chanyshev, A. (2025b). Olivine-ahrensite phase relations in the Mg_2SiO_4-Fe_2SiO_4 system as a function of temperature [Software]. *Zenodo*. https://doi.org/10.5281/zenodo.17649176

Chanyshev, A., Bondar, D., Fei, H., Purevjav, N., Ishii, T., Nishida, K., et al. (2021). Determination of phase relations of the olivine–ahrensite transition in the Mg_2SiO_4-Fe_2SiO_4 system at 1740 K using modern multi-anvil techniques. *Contributions to Mineralogy and Petrology*, *176*, 1–10. https://doi.org/10.1007/s00410-021-01829-x

Chanyshev, A., Ishii, T., Bondar, D., Bhat, S., Kim, E. J., Farla, R., et al. (2022). Depressed 660-km discontinuity caused by akimotoite–bridgmanite transition. *Nature*, *601*(7891), 69–73. https://doi.org/10.1038/s41586-021-04157-z

Duffy, T. S., Zha, C.-s., Downs, R. T., Mao, H.-k., & Hemley, R. J. (1995). Elasticity of forsterite to 16 GPa and the composition of the upper mantle. *Nature*, *378*(6553), 170–173. https://doi.org/10.1038/378170a0

Farla, R., Bhat, S., Sonntag, S., Chanyshev, A., Ma, S., Ishii, T., et al. (2022). Extreme conditions research using the large-volume press at the P61B endstation, PETRA III. *Synchrotron Radiation*, *29*(2), 409–423. https://doi.org/10.1107/s1600577522001047

Frost, D. J. (2003). The structure and sharpness of (Mg, Fe)$_2SiO_4$ phase transformations in the transition zone. *Earth and Planetary Science Letters*, *216*(3), 313–328. https://doi.org/10.1016/s0012-821x(03)00533-8

Graham, E., Schwab, J., Sopkin, S., & Takei, H. (1988). The pressure and temperature dependence of the elastic properties of single-crystal fayalite Fe_2SiO_4. *Physics and Chemistry of Minerals*, *16*(2), 186–198. https://doi.org/10.1007/bf00203203

Huang, Q., Schmerr, N. C., King, S. D., Kim, D., Rivoldini, A., Plesa, A.-C., et al. (2022). Seismic detection of a deep mantle discontinuity within Mars by InSight. *Proceedings of the National Academy of Sciences*, *119*(42), e2204474119. https://doi.org/10.1073/pnas.2204474119

Ishii, T., Huang, R., Myhill, R., Fei, H., Koemets, I., Liu, Z., et al. (2019). Sharp 660-km discontinuity controlled by extremely narrow binary post-spinel transition. *Nature Geoscience*, *12*(10), 869–872. https://doi.org/10.1038/s41561-019-0452-1

Jacobs, M. H., de Jong, B. H., & Oonk, H. A. (2001). The Gibbs energy formulation of α, γ, and liquid Fe_2SiO_4 using Grover, Getting, and Kennedy's empirical relation between volume and bulk modulus. *Geochimica et Cosmochimica Acta*, *65*(22), 4231–4242. https://doi.org/10.1016/s0016-7037(01)00694-9

Katsura, T., Shatskiy, A., Manthilake, M. G. M., Zhai, S., Fukui, H., Yamazaki, D., et al. (2009). Thermal expansion of forsterite at high pressures determined by in situ X-ray diffraction: The adiabatic geotherm in the upper mantle. *Physics of the Earth and Planetary Interiors*, *174*(1–4), 86–92. https://doi.org/10.1016/j.pepi.2008.08.002

Katsura, T., Ueda, A., Ito, E., & Morooka, K. (1998). Postspinel transition in Fe_2SiO_4. In M. H. Manghnani & T. Yagi (Eds.), *High pressure–temperature research: Properties of earth and planetary materials* (pp. 435–440). American Geophysical Union.

Katsura, T., Yokoshi, S., Song, M., Kawabe, K., Tsujimura, T., Kubo, A., et al. (2004). Thermal expansion of Mg_2SiO_4 ringwoodite at high pressures. *Journal of Geophysical Research*, *109*(B12), B12209. https://doi.org/10.1029/2004jb003094

Khan, A., Liebske, C., Rozel, A., Rivoldini, A., Nimmo, F., Connolly, J., et al. (2018). A geophysical perspective on the bulk composition of Mars. *Journal of Geophysical Research: Planets*, *123*(2), 575–611. https://doi.org/10.1002/2017je005371

Khan, A., Sossi, P. A., Liebske, C., Rivoldini, A., & Giardini, D. (2022). Geophysical and cosmochemical evidence for a volatile-rich Mars. *Earth and Planetary Science Letters*, *578*, 117330. https://doi.org/10.1016/j.epsl.2021.117330

Kumazawa, M., & Anderson, O. L. (1969). Elastic moduli, pressure derivatives, and temperature derivatives of single-crystal olivine and single-crystal forsterite. *Journal of Geophysical Research*, *74*(25), 5961–5972. https://doi.org/10.1029/jb074i025p05961

Liu, Q., Liu, W., Whitaker, M. L., Wang, L., & Li, B. (2008). Compressional and shear wave velocities of Fe_2SiO_4 spinel at high pressure and high temperature. *High Pressure Research*, *28*(3), 405–413. https://doi.org/10.1080/08957950802296287

Ma, C., Tschauner, O., Beckett, J. R., Liu, Y., Rossman, G. R., Sinogeikin, S. V., et al. (2016). Ahrensite, γ-Fe_2SiO_4, a new shock-metamorphic mineral from the Tissint meteorite: Implications for the Tissint shock event on Mars. *Geochimica et Cosmochimica Acta*, *184*, 240–256. https://doi.org/10.1016/j.gca.2016.04.042

Matsui, M., Katsura, T., Kuwata, A., Hagiya, K., Tomioka, N., Sugita, M., et al. (2006). Equation of state of $(Mg_{0.8}, Fe_{0.2})_2SiO_4$ ringwoodite from synchrotron X-ray diffraction up to 20 GPa and 1700 K. *European Journal of Mineralogy*, *18*(5), 523–528. https://doi.org/10.1127/0935-1221/2006/0018-0523

McCammon, C., Frost, D., Smyth, J., Laustsen, H., Kawamoto, T., Ross, N., & Van Aken, P. (2004). Oxidation state of iron in hydrous mantle phases: Implications for subduction and mantle oxygen fugacity. *Physics of the Earth and Planetary Interiors*, *143*, 157–169. https://doi.org/10.1016/j.pepi.2003.08.009

McDonough, W. F., & Sun, S.-S. (1995). The composition of the Earth. *Chemical Geology*, *120*(3–4), 223–253. https://doi.org/10.1016/0009-2541(94)00140-4

Miyahara, M., Ohtani, E., Kimura, M., El Goresy, A., Ozawa, S., Nagase, T., et al. (2010). Coherent and subsequent incoherent ringwoodite growth in olivine of shocked L6 chondrites. *Earth and Planetary Science Letters*, *295*(1–2), 321–327. https://doi.org/10.1016/j.epsl.2010.04.023

Nishihara, Y., Doi, S., Kakizawa, S., Higo, Y., & Tange, Y. (2020). Effect of pressure on temperature measurements using WRe thermocouple and its geophysical impact. *Physics of the Earth and Planetary Interiors*, *298*, 106348. https://doi.org/10.1016/j.pepi.2019.106348

Pittarello, L., Ji, G., Yamaguchi, A., Schryvers, D., Debaille, V., & Claeys, P. (2015). From olivine to ringwoodite: A TEM study of a complex process. *Meteoritics & Planetary Science*, *50*(5), 944–957. https://doi.org/10.1111/maps.12441

Ringwood, A. (1958). The constitution of the mantle—II: Further data on the olivine-spinel transition. *Geochimica et Cosmochimica Acta*, *15*(1–2), 18–29. https://doi.org/10.1016/0016-7037(58)90005-x

Sharp, T. G., & DeCarli, P. S. (2006). Shock effects in meteorites. *Meteorites and the Early Solar System II*, *943*, 653–677.

Sharp, T. G., Walton, E. L., Hu, J., & Agee, C. (2019). Shock conditions recorded in NWA 8159 Martian augite basalt with implications for the impact cratering history on Mars. *Geochimica et Cosmochimica Acta*, *246*, 197–212. https://doi.org/10.1016/j.gca.2018.11.014

Tange, Y., Nishihara, Y., & Tsuchiya, T. (2009). Unified analyses for P-V-T equation of state of MgO: A solution for pressure-scale problems in high P-T experiments. *Journal of Geophysical Research*, *114*(B3). https://doi.org/10.1029/2008jb005813

Taylor, G. J. (2013). The bulk composition of Mars. *Geochemistry*, *73*(4), 401–420. https://doi.org/10.1016/j.chemer.2013.09.006

Walton, E. L., & McCarthy, S. (2017). Mechanisms of ringwoodite formation in shocked meteorites: Evidence from L5 chondrite Dhofar 1970. *Meteoritics & Planetary Science*, *52*(4), 762–776. https://doi.org/10.1111/maps.12829

Wang, F., Bausch, H. J., Gardner, L. L., Zhang, D., Armstrong, K., Bell, A. S., et al. (2025). Thermoelastic properties of iron-rich ringwoodite and the deep mantle aerotherm of Mars. *Geophysical Research Letters*, *52*(3), e2024GL109666. https://doi.org/10.1029/2024gl109666

Xie, L., Yoneda, A., Liu, Z., Nishida, K., & Katsura, T. (2020). Boron-doped diamond synthesized by chemical vapor deposition as a heating element in a multi-anvil apparatus. *High Pressure Research*, *40*(3), 369–378. https://doi.org/10.1080/08957959.2020.1789618

Xie, L., Yoneda, A., Yoshino, T., Yamazaki, D., Tsujino, N., Higo, Y., et al. (2017). Synthesis of boron-doped diamond and its application as a heating material in a multi-anvil high-pressure apparatus. *Review of Scientific Instruments*, *88*(9), 093904. https://doi.org/10.1063/1.4993959

Yoshizaki, T., & McDonough, W. F. (2020). The composition of Mars. *Geochimica et Cosmochimica Acta*, *273*, 137–162. https://doi.org/10.1016/j.gca.2020.01.011